Design Robust Cascade Control Structure for Voltage Source Converters

Yi Zhou, *Student Member, IEEE*, Zhixin Miao, *Senior Member, IEEE*, Yin Li, *Student Member, IEEE*, Lingling Fan, *Senior Member, IEEE*

***Abstract*—This paper proposes a novel robust cascade structure which has better performance when the transmission line undergoes a perturbation. Cascade control structure is normally used when the control procedure can be split into two (or more) cascaded parts. Compared with the conventional cascade control structure which has a limited ability to handle the perturbation in the plant model, the novel structure has better robustness when the transmission line inductance varies. After introducing their structures, the poles and zeros of the closed-loop system related to the conventional and the robust cascade structures will be generated and used to analyze their stability. To verify the theoretical analysis, both cascade structures are applied to a voltage source converter (VSC) and are simulated in MATLAB/Simulink. The different step responses are plotted and analyzed with increasing the transmission line inductance.**

***Index Terms*—Cascade control, robust structure, P/Q controlled VSC**

I. Introduction

A microgrid system contains several distributed and interconnected generator units, loads and energy storage units [1]. With more and more Distributed Generations (DGs) installed, the efficiency and reliability of power system have been improved because DG systems can share stresses on power transmission and distribution infrastructure [2], [3].

In DG systems, voltage source converters play an important role in high quality power transfer. VSCs are widely used to integrate DG systems to the utility power grid or to drive the loads. A VSC usually has inner loops to control the currents while its outer loops are designed based on the control objectives such as real and reactive power control (P/Q) and Voltage/Frequency (V/F) [4]–[8]. To connect a VSC-based DG to the grid, P/Q control is usually utilized. Cascade structure is very popular when the control process can be split into the inner loop and the outer loop. With the two distinct bandwidths, inner loop compensator and outer loop compensator need to be designed sequentially. Inner loop is designed based on the plant model first; then, the outer loop is designed based on the inner closed-loop transfer function [9]. However, if the inner closed-loop transfer function is changed, the outer loop stability can not be guaranteed. In another word, the design of the conventional controllers is strongly dependent on the plant model of the specific circuit. Therefore, if the plant model is changed because of any perturbation in the circuit, this system may become unstable. For example, the transmission line is necessarily required to connect the DG to the grid and its inductance is variable dependent on its length. When the inductance is out of the acceptable range, the conventional control control loop will not make the system stable. The system may have over voltage or oscillation problems to damage the system.

Y. Zhou, Z. Miao, Y. Li, and L. Fan are with Dept. of Electrical Engineering, University of South Florida, Tampa FL 33620. Email: zmiao@usf.edu.

Power electronics and control technology are improved towards to increase the performance, robustness, and reliability [2], [8], [10], [11]. Therefore, in order to deal with the uncertain change of the inductance of the transmission line, a robust control system is very necessary. The robust cascade structure proposed in [9] with an application in chemical process control is analyzed and implemented to a VSC with P/Q control in this paper. This structure can handle inductance increasing of the transmission line. With this novel robust cascade control structure, the DG system robustness can be enhanced by minimizing the mutual influence among the cascaded loops.

The rest of the paper is organized as follows: Section II will present the structures of the conventional cascade system and stability analysis using transfer function and the pole-zero map. Section III presents the robust cascade system. In Section IV, the simulation results of the conventional and robust cascade structures will be plotted and compared to verify the theoretical analysis in Section II and III. Section V is the conclusion.

II. Conventional Cascade Structure used in P/Q control

A. Overall structure of the VSC circuit with P/Q control

Fig. 1 shows the structure of the grid-imposed frequency VSC circuit with P/Q control. The control objective is to control the real power and reactive power at the point of common coupling (PCC). When the DG system connects to the grid, the voltage and frequency at PCC point are fixed. Because the control loop design is in $(d+jq)$-frame, phase-locked loop (PLL) is used to achieve a synchronization.

With this configuration, the differential equations of the currents through the transmission line can be expressed as:

$$\begin{aligned} L\frac{di_d}{dt} &= -(R+R_{on})i_d + L\omega i_q + V_{td} - V_{sd}, \\ L\frac{di_q}{dt} &= -(R+R_{on})i_q - L\omega i_d + V_{tq} \end{aligned} \tag{1}$$

After decoupling the speed voltage part and transfer (1) from time domain to Laplace domain, inner loop plant model

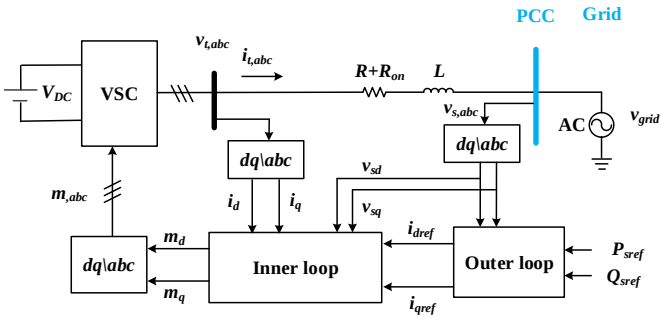

Fig. 1: Overall structure of the VSC circuit with P/Q control.

$H(s)$ can be found using (2).

$$\begin{aligned} i_d(s) &= \frac{1}{Ls+R+R_{on}} u_{id}(s) \\ i_q(s) &= \frac{1}{Ls+R+R_{on}} u_{iq}(s) \end{aligned} \tag{2}$$

where u_{id} and u_{iq} are the intermediate signals which are defined as:

$$\begin{aligned} u_{id} &= -L\omega i_q + V_{td} - V_{sd} \\ u_{iq} &= L\omega i_d + V_{tq} - V_{sq} \end{aligned} \tag{3}$$

Hence, $H(s)$ is $\frac{1}{Ls+R+R_{on}}$ and its outputs are $i_d(s)$ and $i_q(s)$. Define the outer loop plant model as $G(s)$ whose inputs are $i_d(s)$ and $i_q(s)$ and outputs of $G(s)$ are P and Q. Hence, $G(s)$ is a constant gain, $\frac{3}{2}V_{sd}$, based on the following equations (4).

$$\begin{aligned} S &= VI^* = \sqrt{\frac{3}{2}}(v_{sd} - jv_{sq})\sqrt{\frac{3}{2}}(i_d + ji_q) \\ P &= \frac{3}{2}v_{sd}i_d \\ Q &= -\frac{3}{2}v_{sd}i_q \end{aligned} \tag{4}$$

B. Conventional cascade structure

A typical conventional cascade control structure is shown in Fig. 2. In this figure, there are two loops, the inner loop $F_1(s)$ and the outer loop $F_2(s)$. $H(s)$ and $G(s)$ are the plant models of $F_1(s)$ and $F_2(s)$ respectively. $R_1(s)$ and $R_2(s)$ are the corresponding compensators. $y^0(t)$ and $y(t)$ are the input and output of the system. $w(t)$, $u(t)$ and $v(t)$ are the intermediate signals in time domain. Their Laplace representations can be defined as $Y^0(s)$, $Y(s)$, $W(s)$, $U(s)$, and $V(s)$.

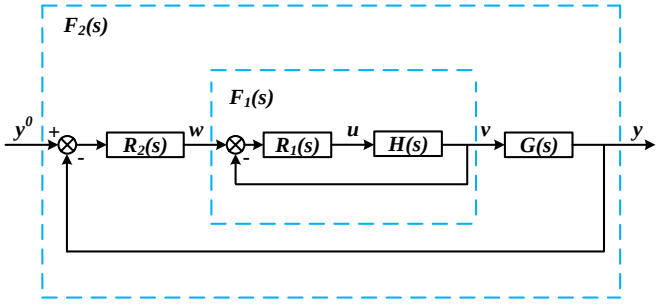

Fig. 2: Block diagram of the conventional cascade structure.

Two compensators, $R_1(s)$ and $R_2(s)$, need to be designed sequentially [12], [13]. Since the inner loop and outer loop are independent with each other, the conventional control design philosophy is to design the inner loop compensator first. When the inner loop can track the reference, the outer loop compensator is then designed. The bandwidth of the outer loop should be smaller than the inner loop so the inner loop $F_1(s)$ will reach steady state very fast. With this design philosophy, the interaction between the inner loop and the outer loop is minimized.

It is assumed that plant models of the inner loop and the outer loop are time-invariant single-input-single-output (SISO) linear systems. Hence, the outputs of the inner loop and outer loop, $Y(s)$ and $V(s)$, can be represented as:

$$\begin{aligned} Y(s) &= G(s)V(s) \\ V(s) &= H(s)U(s) \end{aligned} \tag{5}$$

Then, the inner closed-loop transfer function $F_1(s)$ is derived as:

$$F_1(s) = \frac{V(s)}{W(s)} = \frac{R_1(s)H(s)}{1+R_1(s)H(s)} \tag{6}$$

Because the inner loop has much faster dynamics than the outer loop, $F_1(s)$ is considered as 1. This condition is claimed as the ideal condition. Under the ideal condition, $F_{2i}(s)$ can be assigned initially to the transfer function $F_2(s)$ so the closed-loop transfer function of the whole cascade structure is:

$$\begin{aligned} F_2(s) &= \frac{Y(s)}{Y^0(s)} = F_{2i}(s) \\ &= \frac{R_{2i}(s)G(s)}{1+R_{2i}(s)G(s)} \end{aligned} \tag{7}$$

where R_{2i} is the ideal compensator.

After converting (7), the transfer function of the outer loop compensator $R_2(s)$ is obtained.

$$R_2(s) = R_{2i}(s) = \frac{F_{2i}(s)}{G(s)(1-F_{2i}(s))} \tag{8}$$

With inductance increasing, the transfer function of the inner loop will be changed. It makes the dynamics of the inner loop slower. In another word, the system will not be under the ideal condition. To keep $W(s)/Y^0(s)$ remain the same as in the ideal case, the compensator under the non-ideal condition $R_{2r}(s)$ needs to be rewritten as:

$$R_2(s) = R_{2r}(s) = \frac{R_{2i}(s)}{1+R_{2i}(s)G(s)(1-F_1(s))} \tag{9}$$

If $F_1(s)$ undergoes a perturbation, the closed-loop transfer function of the conventional cascade structure will be $F_{2r}(s)$ rather than $F_{2i}(s)$.

$$F_2(s) = F_{2r}(s) = \frac{R_2(s)F_{1p}(s)G(s)}{1+R_2(s)F_{1p}(s)G(s)} \tag{10}$$

where $F_{1p}(s)$ is $F_1(s)$ with a perturbation.

Substituting (9) into (10) and simplifying it,

$$F_2(s) = F_{2r}(s) = \frac{F_{2i}(s)F_{1p}(s)}{1+F_{2i}(s)(F_{1p}(s)-F_1(s))} \tag{11}$$

After obtaining the closed-loop transfer function for the conventional cascade structure in Fig. 2, we can find the locations of poles and zeros by providing the specific parameters. The used parameters are listed in Table I and the used detailed equations are (12). If the inductance L is increased while other parameters keep the same, multiple poles will be plotted in one figure to generate the pole-zero map shown in Fig. 3. Along with the transmission line inductance L raising from 100 μH to 900 μH, the four poles are moving forward to the imaginary axis, even to the right half plane (RHP). It clearly shows that the system should be unstable when L =900 μH because of the poles dropped on RHP.

$$
\begin{aligned}
H(s) &= \frac{1}{Ls + R + Ron} \\
G(s) &= \frac{3\sqrt{2}}{2\sqrt{3}} V_{grid} \\
F_1(s) &= \frac{R_1 \frac{1}{Ls+R+R_{on}}}{1 + R_1 \frac{1}{Ls+R+R_{on}}} \\
F_2(s) &= \frac{R_2 F_1(s) G(s)}{1 + R_2 F_1(s) G(s)}
\end{aligned}
\tag{12}
$$

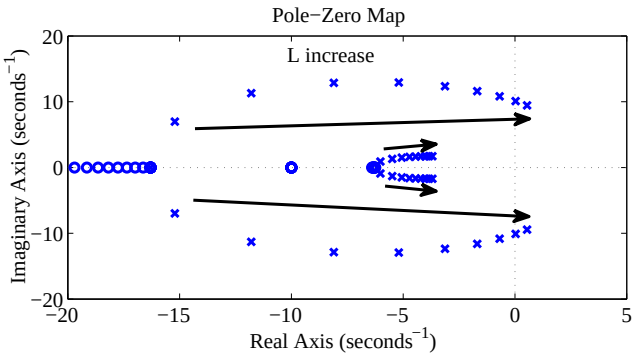

Fig. 3: Pole-zero map of the conventional cascade structure.

C. P/Q control loop using the conventional cascade structure

The aforementioned subsection analyzed the stability of the conventional cascade structure using simplified block diagram and transfer functions. If we apply this structure to the VSC circuit with P/Q control, the control diagram should be designed like Fig. 4.

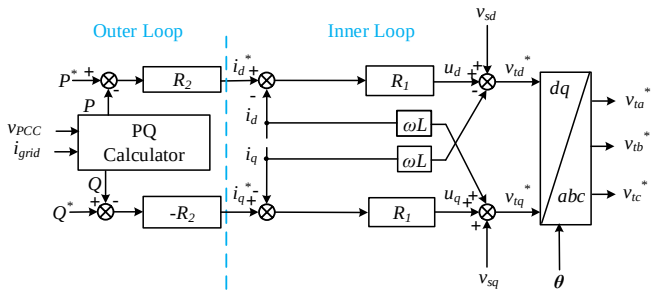

Fig. 4: P/Q control diagram with the conventional cascade control.

θ is generated by a PLL with inputs from PCC voltage V_s. Because the inner loop bandwidth is sufficiently larger than the outer loop bandwidth, the speed of the overall system dynamics is dependent on the outer loop. P/Q outer loop can be designed according to the classical design criteria. However, if a large variation happens in the inner loop plant model, especially if the inductor size is increased, the conventional cascade structure can not make the system stable.

III. Robust Cascade Structure used in P/Q Control

The robust cascade structure is analyzed based on the same VSC circuit shown in Fig. 1, so the circuit will not be introduced in this section.

A. Robust cascade structure

Fig. 5 shows the robust cascade structure of cascade control. The most obvious difference is that the robust cascade structure has one more feedback loop. The inner loop does not change. Therefore, only the new feedback compensator $R_4(s)$ and the outer loop compensator $R_3(s)$ should be redesigned. They are expressed by the following:

$$
\begin{aligned}
R_3(s) &= \frac{F_{2i}(s)}{G(s)} \\
R_4(s) &= F_{2i}(s)
\end{aligned}
\tag{13}
$$

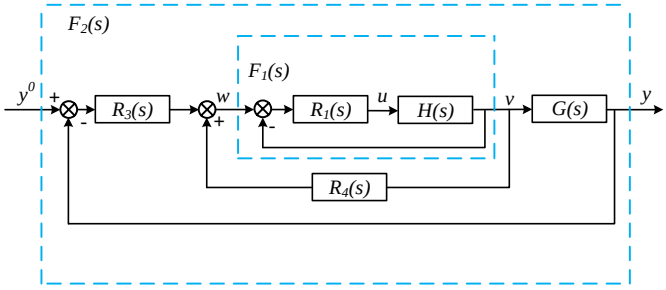

Fig. 5: Block diagram of the robust cascade structure.

For the robust cascade structure, if $F_1(s)$ undergoes a perturbation, the new transfer function of the inner loop with R_4 is $\frac{F_{1p}(s)}{1-R_4(s)F_{1p}(s)}$. After replacing $F_1(s)$ using the new inner loop transfer function, the transfer function of the whole robust cascade structure is expressed as:

$$
F_2(s) = F_{2r}(s) = \frac{\frac{R_3(s)F_{1p}(s)G(s)}{1-R_4(s)F_{1p}(s)}}{1 + \frac{R_3(s)F_{1p}(s)G(s)}{1-R_4(s)F_{1p}(s)}} \tag{14}
$$

Substituting $R_3(s)$ and $R_4(s)$ into 14,

$$
\begin{aligned}
F_2(s) = F_{2r} &= \frac{\frac{F_{2i}(s)F_{1p}(s)G(s)}{G(s)}}{1 - F_{2i}(s)F_{1p}(s) + \frac{F_{2i}(s)G(s)F_1(s)}{G(s)}} \\
&= F_{2i}(s)F_{1p}(s)
\end{aligned}
\tag{15}
$$

Equation (15) clearly shows that the robust structure is asymptotically stable as long as $F_{1p}(s)$ and $F_{2i}(s)$ are asymptotically stable. The inner loop of the robust cascade structure

is the same as that of the conventional cascade structure while their outer loops are different. Therefore, $F_1(s)$, $H(s)$, and $G(s)$ in (12) can be used for this structure while $F_2(s)$ needs to be rewritten as (16). The parameters used for the robust cascade structure are from Table I, too.

$$F_2(s) = \frac{R_3 \frac{F_1(s)}{1-R_4F_1(s)} G(s)}{1 + R_3 \frac{F_1(s)}{1-R_4F_1(s)} G(s)} \tag{16}$$

Based on (16), the pole-zero map of the robust cascade structure can be mapped with the same method. Fig. 6 shows the pole-zero map of the robust cascade structure shown in Fig. 5. Like Fig. 3, the two poles are moving forward to the imaginary axis with increasing transmission line inductance L from 100 μH to 900 μH. However, the poles keep in left half plan (LHP) even if L =900 μH. It is concluded that the novel robust cascade structure improves the robustness of the cascaded structure control.

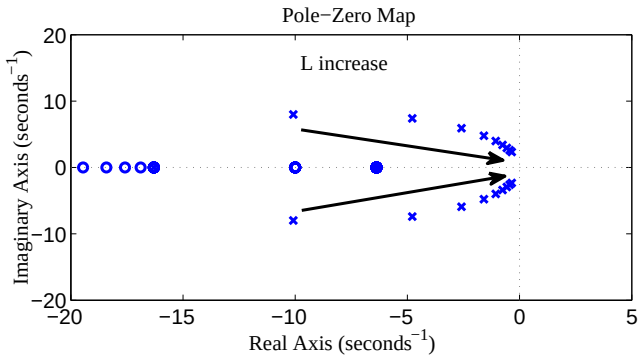

Fig. 6: Pole-zero map of the robust cascade structure.

B. P/Q control loop using the robust cascade structure

Fig. 7 shows the P/Q control diagram with the robust cascade structure. The robust cascade structure has a feedback compensator R_4 and a new R_3 so the control diagram is improved using these two compensators. Fig. 4 and Fig. 7 are used to build the average models in MATLAB/Simulink.

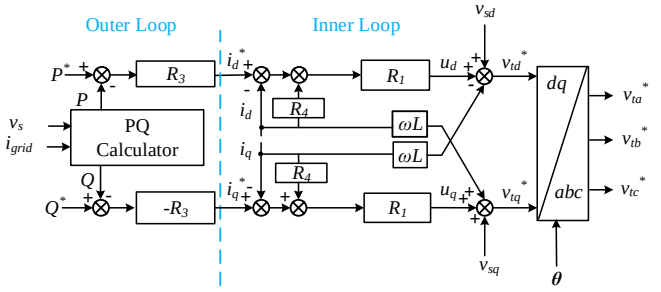

Fig. 7: P/Q control diagram with the robust cascade control.

IV. Case Study

To compare the performances of both cascade structures, two average models were built based on Fig. 1 and simulated in Matlab/Simulink. They were corresponding to both of the conventional and robust cascade structures. The parameters used in the average models are from [11] and listed in Table I.

TABLE I: Parameter Initial Settings of P/Q Controlled VSC.

Parameter	Values
V_{DC}	1250 V
V_{grid}	480 V
L	100 μH
$R + R_{on}$	1.63 mΩ
Carrier frequency f_s	3420 Hz
τ_i	2.0 ms
R_1	$\frac{0.05s+0.815}{s}$
R_2	$\frac{0.003s+0.03}{s}$
R_3	$\frac{0.001086s+0.01086}{s}$
R_4	$\frac{0.6386s+6.386}{s}$

The total simulation time is 100 seconds and there were two events happened during it. The real power reference P^* was increased from 500 kW to 700 kW at 40 second while the reactive power reference Q^* was increased from 0 to 150 kVAr at 70 second. The reference values were plotted by the red dotted lines in Fig. 8 and Fig. 9. The simulation results were plotted by the solid blue lines in figures to show the step responses of P and Q.

According to Fig. 3 and Fig. 6, the critical eigenvalues of the conventional cascade structure are -6.405 and -1373.3 when L =100 μH; the critical eigenvalues of the robust cascade structure are -6.3767 and -499.4238 with the same L. Hence, the theoretical analysis proves that both of the cascade structures can make the system stable if L =100 μH. The first rows of Fig. 8 and Fig. 9 verified it. In addition, the perfect reference tracking on P and Q can indicate that the control objective was achieved by both of structures.

Besides the initial value of the transmission line inductance, another three different values of L were selected, 500 μH, 860 μH, and 900 μH. Based on the pole-zero map, they can cause the conventional cascade structure system under three different stability levels, small oscillation, large oscillation, and unstable. All of three stability levels can also be verified by the left columns of Fig. 8 and Fig. 9. For example, when L =900 μH, two critical eigenvalues of the conventional cascade structure are $0.0316 \pm 10.0988i$, which are located on RHP shown in Fig. 3 so the system should be unstable. In its corresponding plots, the left lowest plots of Fig. 8 and Fig. 9, the oscillations of the step responses became larger and larger so the system could not return to steady state anymore. For another example, when L =860 μH, two critical poles are very closed to the imaginary axis and the damping is 0.0214 at those locations. In another word, the step responses

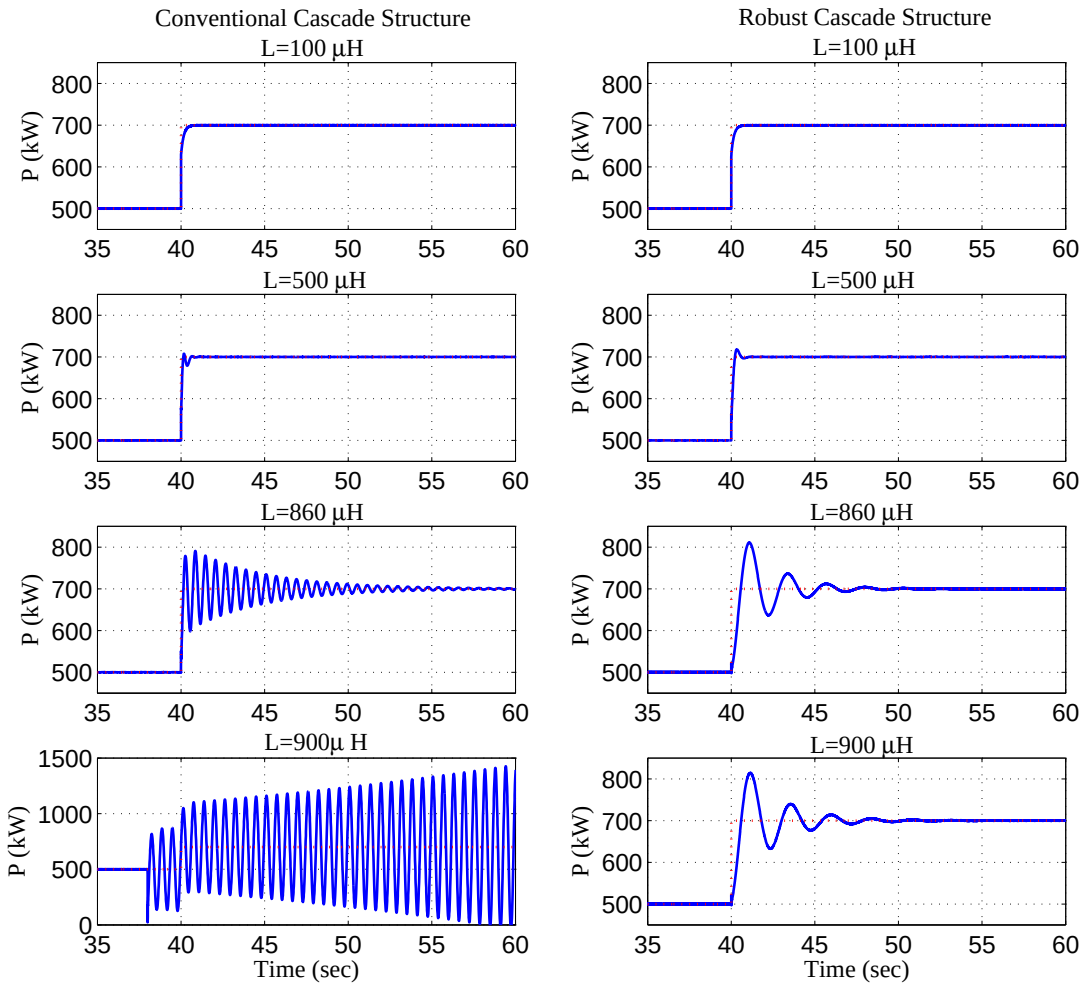

Fig. 8: The step responses of P corresponding to different L. The left column is related to the conventional cascade structure while the right column is related to the robust one. Red dotted line is the reference.

in the conventional cascade structure should have the obvious oscillations when L =860 μH. Actually, the corresponding plots in Fig. 8 and FIg. 9 showed the large oscillations.

Now, let's compare the left columns and right columns of Fig. 8 and Fig. 9. The left columns are related to the conventional cascade structure and the right columns are related to the robust one. Both of them had the very similar step responses when L was relative small shown in the first row of Fig. 8 and Fig. 9. However, when L was increased to 860 μH, the step responses of the conventional structure had the obvious oscillations while the robust one only had a few oscillations. Furthermore, although the conventional one became unstable, the robust cascade structure kept stable and its step responses still remained a few oscillations when L =900 μH. According to these two figures, it is concluded that the robust cascade structure can make the system stable within the large range of the transmission line inductance. In another word, the robust cascade structure improves the robustness of VSC circuit with the P/Q control.

V. Conclusion

It is the first time to design the robust cascade structure for the VSC circuit with P/Q control. After analyzing the stability of the conventional and robust cascade structures using the pole-zero maps of the closed-loop systems, we can claim that the robust cascade structure can make the VSC circuit with P/Q control have better robustness on the transmission line inductance. The simulation results from the average models verify the theoretical analysis. Oscillations can be observed obviously in the step responses from the conventional model with inductance increasing while the simulation results from the robust model had much better performance. Therefore, the robust cascade structure has a great potential in VSC control.

References

[1] H. Gndz, . Snmez, and S. Ayasun, "Comprehensive gain and phase margins based stability analysis of micro-grid frequency control system with constant communication time delays," *IET Generation, Transmission Distribution*, vol. 11, no. 3, pp. 719–729, 2017.

[2] G. Chicco and P. Mancarella, "Distributed multi-generation: a comprehensive view," *Renewable and Sustainable Energy Reviews*, vol. 13, no. 3, pp. 535–551, 2009.

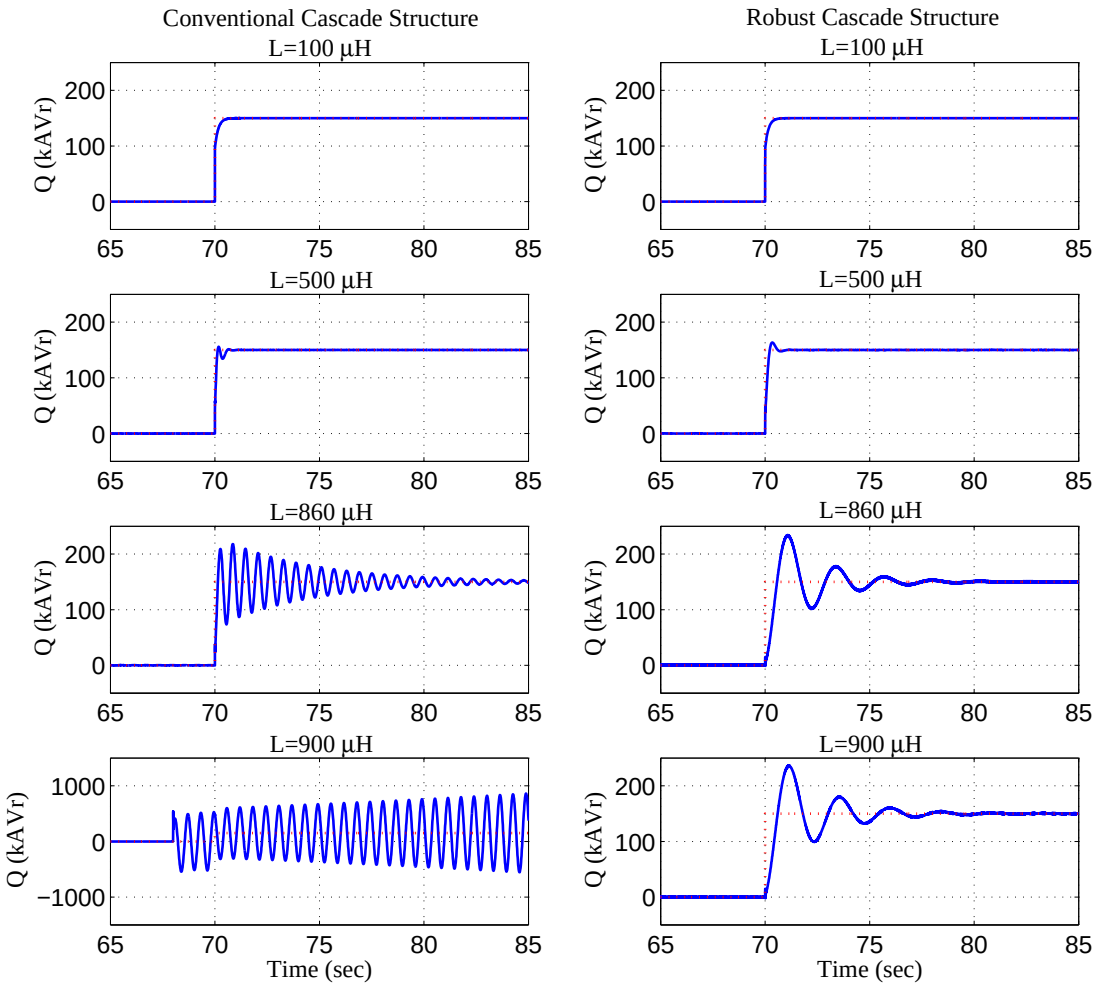

Fig. 9: The step responses of Q corresponding to different L. The left column is related to the conventional cascade structure while the right column is related to the robust one. Red dotted line is the reference.

[3] S. Yang, Q. Lei, F. Z. Peng, and Z. Qian, "A robust control scheme for grid-connected voltage-source inverters," *IEEE Transactions on Industrial Electronics*, vol. 58, no. 1, pp. 202–212, Jan 2011.

[4] F. Blaabjerg, F. Iov, Z. Chen, and K. Ma, "Power electronics and controls for wind turbine systems," in *Energy Conference and Exhibition (EnergyCon), 2010 IEEE International*, Dec 2010, pp. 333–344.

[5] J. Dixon, L. Moran, J. Rodriguez, and R. Domke, "Reactive power compensation technologies: State-of-the-art review," *Proceedings of the IEEE*, vol. 93, no. 12, pp. 2144–2164, Dec 2005.

[6] C. A. Caizares, M. Pozzi, S. Corsi, and E. Uzunovic, "{STATCOM} modeling for voltage and angle stability studies," *International Journal of Electrical Power and Energy Systems*, vol. 25, no. 6, pp. 431 – 441, 2003. [Online]. Available: http://www.sciencedirect.com/science/article/pii/S0142061502001254

[7] H. Ghasemi and C. A. Canizares, "Validation of a statcom transient stability model through small-disturbance stability studies," in *System of Systems Engineering, 2007. SoSE '07. IEEE International Conference on*, April 2007, pp. 1–6.

[8] A. Llaria, O. Curea, J. Jiménez, and H. Camblong, "Survey on microgrids: unplanned islanding and related inverter control techniques," *Renewable energy*, vol. 36, no. 8, pp. 2052–2061, 2011.

[9] C. Maffezzoni, N. Schiavoni, and G. Ferretti, "Robust design of cascade control," *IEEE Control Systems Magazine*, vol. 10, no. 1, pp. 21–25, 1990.

[10] A. M. Bouzid, J. M. Guerrero, A. Cheriti, M. Bouhamida, P. Sicard, and M. Benghanem, "A survey on control of electric power distributed generation systems for microgrid applications," *Renewable and Sustainable Energy Reviews*, vol. 44, pp. 751–766, 2015.

[11] A. Yazdani and R. Iravani, *Voltage-sourced converters in power systems: modeling, control, and applications*. John Wiley & Sons, 2010.

[12] J. J. d'Azzo and C. D. Houpis, *Linear control system analysis and design: conventional and modern*. McGraw-Hill Higher Education, 1995.

[13] N. S. Nise, *Control Systems Engineering*, 3rd ed. New York, NY, USA: John Wiley & Sons, Inc., 2000.